Polypeptide/Doxorubicin Hydrochloride Polymersomes Prepared Through Organic Solvent-free Technique as a Smart Drug Delivery Platform

Mingqiang Li, Shixian Lv, Zhaohui Tang, Wantong Song, Haiyang Yu, Hai Sun, Huaiyu Liu,* Xuesi Chen*

Rapid and efficient side-chain functionalization of polypeptide with neighboring carboxyl-groups is achieved via the combination of ring-opening polymerization and subsequent thiol-yne click chemistry. The spontaneous formation of polymersomes with uniform size is found to occur in aqueous medium via electrostatic interaction between the anionic polypeptide and cationic doxorubicin hydrochloride (DOX·HCl). The polymersomes are taken up by A549 cells via endocytosis, with a slightly lower cytotoxicity compared with free DOX·HCl. Moreover, the drug-loaded polymersomes exhibit the enhanced therapeutic efficacy, increase apoptosis in tumor tissues, and reduce systemic toxicity in nude mice bearing A549 lung cancer xenograft, in comparison with free DOX·HCl.

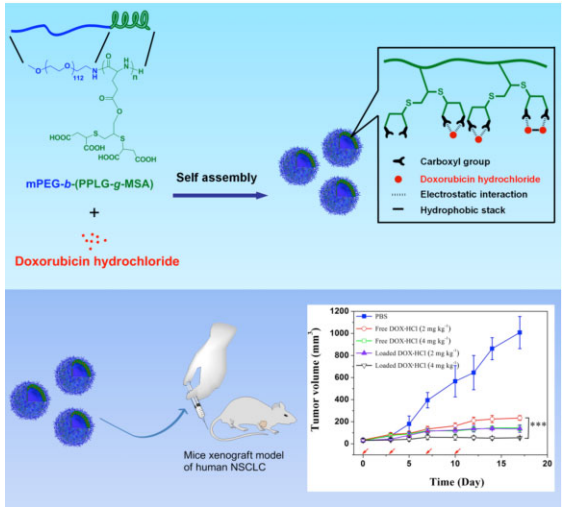

1. Introduction

Polypeptide-based copolymers have attracted considerable attention due to their excellent biocompatibility, biodegradability, and precise secondary conformations, making them highly desirable for anticancer drug delivery.[1] The most common approach to prepare the polypeptide-based copolymers involves the well-studied primary-amine-initiated ring-opening polymerization (ROP) of *N*-carboxyanhydrides (NCAs), which can accommodate a wide range of monomers containing various functional groups.[2] However, when the polypeptides with functional amino (e.g., lysine), carboxylic (e.g., aspartate and glutamate), or sulfydryl (e.g., cysteine) groups were prepared, the multiple selective protection and deprotection steps are often required.[3] Side-chain functionalized polypeptides, which have a broad application in the biomedical researches, are primarily obtained via acylation-mediated amidation or esterification, and carbodiimide-activated coupling (amidation or esterification) of a well-defined polypeptide

M. Li, S. Lv, Z. Tang, W. Song, H. Yu, H. Sun, X. Chen
Key Laboratory of Polymer Ecomaterials, Changchun Institute of Applied Chemistry, Chinese Academy of Sciences, Changchun, 130022, P. R. China
E-mail: xschen@ciac.ac.cn
M. Li, S. Lv, W. Song
University of Chinese Academy of Sciences, Beijing, 100039, P. R. China
H. Liu
Laboratory Animal Center, Jilin University, Changchun, 130012, P. R. China
E-mail: liuhuaiyu@jlu.edu.cn

[a]**Supporting Information** is available at Wiley Online Library or from the author.

© 2013 WILEY-VCH Verlag GmbH & Co. KGaA, Weinheim

DOI: 10.1002/mabi.201300222

precursor.[4] Recently, we reported a novel and efficient approach to synthesize polypeptide containing various pendant functional groups (e.g., glucose, galactose, mannose, oligo(ethylene glycol)s, and azide end-functionalized poly(2-aminoethyl methacrylate hydrochloride) through the introduction of a new polymer, poly(γ-propargyl-L-glutamate) (PPLG), which contained "clickable" alkyne pendants that could be reacted with an azide via the copper-catalyzed azide-alkyne Huisgen 1,3-dipolar cycloaddition reaction.[5] This synthetic strategy was allowed for the convenient and efficient functionalization of a polypeptide without protection and deprotection steps. However, the long reaction times and high reaction temperatures, in particular for macromolecular systems, might be a limitation of this technique.[6] On the other hand, residual copper catalyst may cause potential deleterious effects and hamper the subsequent biological applications.[7]

The radical-mediated thiol-ene click reaction is an attractive copper-free route that allows one to functionalize the polypeptide segments, which has been reported in recent years.[8] Similar to the thiol-ene reaction, the thiol-yne photoreaction proceeds rapidly and efficiently under ambient conditions without the use of a metal catalyst.[9] The radical mechanism of the thiol-yne reaction makes it a very robust and versatile method that tolerates a variety of functional groups.[10] Hence, it has been a powerful and versatile methodology for materials synthesis. Recently, thiol-yne click chemistry has been reported as a convenient and universal route for peptide conjugation.[11]

Generally, the polypeptide-based drug carrier consists of hydrophilic poly(ethylene glycol) (PEG) and hydrophobically derivatized polypeptide block, served as either a reservoir within which hydrophobic drugs (e.g., paclitaxel, doxorubicin, and amphotericin B) are encapsulated,[12] or the drugs (e.g., paclitaxel, doxorubicin, and SN 38) are covalently bound to the polymer.[13] However, most of the reported hydrophobic drug encapsulation procedures involve the dissolution of the polymeric carrier and drug in an organic solvent, and the subsequent removal of the organic solvent by either dialysis or solvent evaporation.[1,14] The use of organic solvents in pharmaceutical formulations is rarely desirable, owing to their potential deleterious effects and the regulatory requirement to quantify residual levels of harmful organic solvents.[15] If possible, the drug encapsulation procedure should avoid using organic solvent to ensure the safe and effective drug-use for patients. In addition to encapsulate hydrophobic drugs within the interior core of these amphiphilic polymeric micelles, ionic block polymers with good water solubility may also self-assemble into core–shell nanostructures when loaded with oppositely charged components (e.g., lysozyme and siRNA)[16] or platinum (II) antitumor drugs.[17] This is achieved by exploiting the electrostatic or chelate interactions between the ionic polypeptide block of the polymeric carrier and the biological macromolecular drug or platinum (II) antitumor drugs.

Doxorubicin hydrochloride (DOX · HCl), an anthracycline anticancer drug, is a leading clinically used anticancer drug due to its potency and a broad spectrum of activity against diverse cancer types (e.g., breast, lung, prostate, brain, cervix, bone, and bladder cancers).[18] However, the dose-dependent cardiotoxicity, myelosuppression, and development of multidrug resistance associated with unformulated DOX · HCl limit its therapeutic efficacy. Many new and innovative strategies to entrap DOX · HCl in different nanocarriers with a variety of architectures including polymer–drug conjugates, micelles, nanogels, liposomes, dendrimers, and nanospheres have been developed to overcome this limitation. A number of stories involving doxorubicin delivery via hydrophobic interaction between the drug and hydrophobic moieties of the drug carrier have been reported in the past few years.[12b][19] As a general rule, DOX · HCl was neutralized by excess triethylamine to remove the hydrochloride and make doxorubicin hydrophobic in organic solvents (DMF or DMSO).[20] Nevertheless, the trace residual triethylamine and solvent may do harm to the human body. Recently, a few attempts have been made to load hydrophilic DOX · HCl, which is a weak amphipathic base (pK_a 8.3), into anionic polymers through electrostatic interaction in aqueous medium.[21] These anionic polymer/DOX · HCl complexes were relatively stable at neutral pH but dissociate slowly under lower pH analogous to the acidic environment in endosome/lysosome, suggesting that the DOX · HCl-loaded nanocomposites may be suitable for intracellular drug delivery. However, most of the reported anionic polymer/DOX · HCl complexations were based on non-biodegradable polymers (e.g., poly(methacrylic acid) and poly(acrylic acid)) and devoid of in vivo studies.[21b–f] In addition, to the best of our knowledge, polymers with bidentate dicarboxylic ligands had not previously been reported for DOX · HCl encapsulation.

In present work, we developed a bidentate dicarboxylic ligands functionalized polypeptide, methoxy poly(ethylene glycol)-*b*-poly(γ-propargyl-L-glutamate-*g*-mercaptosuccinic acid) (mPEG-*b*-(PPLG-*g*-MSA)), by combining ROP of a clickable monomer of γ-propargyl-L-glutamate NCA (PLG-NCA) and subsequent thiol-yne photochemistry. Polymersomes with uniform size (≈20 nm) were obtained after electrostatic complex between anionic mPEG-*b*-(PPLG-*g*-MSA) and cationic anticancer drug DOX · HCl in aqueous solution. The DOX · HCl-loaded mPEG-*b*-(PPLG-*g*-MSA) polymersomes (mPEG-*b*-(PPLG-*g*-MSA)-DOX · HCl) were evaluated for physicochemical properties, release profile, cellular uptake, in vitro cytotoxicity, hemolytic activity, tissue distribution, and in vivo antitumor efficacy. This DOX-loaded polymersome showed reduced systemic toxicity

© 2013 WILEY-VCH Verlag GmbH & Co. KGaA, Weinheim

and enhanced antitumor efficacy compared with free DOX · HCl, indicating a potential utility in cancer chemotherapy.

2. Experimental Section

2.1. Materials

Poly(ethylene glycol) monomethyl ether (mPEG, $\overline{M}_n = 5000$) and 2,2′-(ethylenedioxy)bis(ethylamine) were purchased from Aldrich and used without further purification. The amino group terminated PEG monomethyl ether (mPEG-NH_2) and PLG-NCA were synthesized as described in our previous works.[4b][5a] Mercaptosuccinic acid (MSA) and 2,2-dimethoxy-2-phenylacetophenone (DMPA) were obtained from Acros organics and Sigma–Aldrich, respectively. DOX · HCl was purchased from Beijing Huafeng United Technology Corporation. 3-(4,5-Dimethyl-thiazol-2-yl)-2,5-diphenyl tetrazolium bromide (MTT) and 4′,6-diamidino-2-phenylindole dihydrochloride (DAPI) were purchased from Sigma and used as received. *N*,*N*-Dimethylformamide (DMF) was stored over calcium hydride (CaH_2) and purified by vacuum distillation with CaH_2. Purified deionized water was prepared by the Milli-Q plus system (Millipore Co., Billerica, MA, USA).

2.2. Measurements

^{1}H NMR spectra were recorded on a Bruker AV 400 NMR spectrometer in CF_3COOD. Fourier transform infrared (FT-IR) spectra were recorded on a Bio-Rad Win-IR instrument using KBr method. Gel permeation chromatography (GPC) analyses of mPEG-*b*-PPLG were conducted on GPC using a series of linear Tskgel Super columns (AW3000 and AW5000) and Water 515 HPLC pump, with OPTILAB DSP Interferometric Refractometer (Wyatt Technology) as the detector. The eluent was DMF containing 0.01 M lithium bromide (LiBr) at a flow rate of 1.0 mL min^{-1} at 50 °C. Monodispersed polystyrene standards were used to generate the calibration curve. GPC analyses of mPEG-*b*-(PPLG-*g*-MSA) were conducted on a Waters 2414 system equipped with Ultrahydrogel linear column and a Waters 2414 refractive index detector (eluent: 0.1 M phosphate buffer (PB), pH 7.4; flow rate: 0.5 mL min^{-1}; temperature: 35 °C; standard: PEG). Zeta potential (ζ-potential) of the DOX · HCl-loaded mPEG-*b*-(PPLG-*g*-MSA) was gauged on a Zeta Potential/BI-90Plus particle size analyzer (Brookhaven, USA). Dynamic laser scattering (DLS) measurement was performed on a WyattQELS instrument with a vertically polarized He–Ne laser (DAWN EOS, Wyatt Technology). The scattering angle was fixed at 90°. Transmission electron microscopy (TEM) measurement was performed on a JEOL JEM-1011 transmission electron microscope with an accelerating voltage of 100 kV.

2.3. Synthesis of mPEG-*b*-PPLG diblock Copolymer

mPEG-*b*-PPLG diblock copolymer was synthesized through one-step ROP of PLG-NCA monomer with mPEG-NH_2 as macroinitiator according to the literature procedure.[5b][22] Typically, PLG-NCA (2.5775 g, 12.20 mmol) was dissolved in 25 mL of dry DMF and introduced into a flame-dried flask, followed by addition of mPEG-NH_2 (2.0333 g, 0.4067 mmol) dissolved in 20 mL of dry DMF. The polymerization was performed at 25 °C for 72 h. Then, the solution was precipitated into excess amount of cold diethyl ether for three times to give the mPEG-*b*-PPLG block copolymers. After dried under vacuum, the final product was obtained as a yellowish solid.

2.4. Synthesis of mPEG-*b*-(PPLG-*g*-MSA) by Thiol-yne Photochemistry

mPEG-*b*-(PPLG-*g*-MSA) was synthesized by "thiol-yne click" photochemistry. Briefly, mPEG-*b*-PPLG (0.2 g, 0.5447 mmol CC) was dissolved in 5 mL DMF and argon gas was bubbled through the solution for 30 min. After MSA (0.8179 g, 5.4470 mmol of thiols) and DMPA (9.0 mg) were introduced into the flask, the reaction mixture was irradiated by UV light (365 nm) for 90 min. The resulting solution was then dialyzed against PB (0.01 M, pH 7.0) and deionized water for 3 d to remove the excess reactants, followed by lyophilization to obtain a yellowish powder.

2.5. Preparation of the DOX · HCl-loaded mPEG-*b*-(PPLG-*g*-MSA) Complexes

mPEG-*b*-(PPLG-*g*-MSA) lyophilized powder was dissolved in deionized water and stirred for 10 min, then adjust pH to 7.4 with a few drops of 0.1 M NaOH. An aqueous solution of DOX · HCl was added dropwise into the polymer solution and the mixture solution was vigorously stirred overnight in the dark. Excess drug was removed by dialysis (MWCO: 3500 g mol^{-1}) against deionized water for 24 h and followed by lyophilization in the dark. For determination of drug loading content (DLC) and drug loading efficiency (DLE), the lyophilized drug-loaded polymeric powder was dissolved in acetonitrile/water (3:7 v/v, pH was adjusted to 3.0 using phosphoric acid) and measured by UV-Vis spectrometer at 480 nm. DLC and DLE were calculated according to the following formula:

$$\text{DLC}\,(\text{wt}\%) = (\text{weight of loaded drug/weight of dug} - \text{loaded polymersomes}) \times 100\%$$

$$\text{DLE}\,(\text{wt}\%) = (\text{weight of loaded drug/weight of feeding drug}) \times 100\%$$

Fluorescein isothiocyanate (FITC)-labeled mPEG-*b*-(PPLG-*g*-MSA)-DOX · HCl was prepared using a modified version of the method published by Ernsting et al.[23] Briefly, 2,2′-(ethylenedioxy) bis(ethylamine) (10.6 mg, 0.072 mmol) was dissolved in DMSO (2.0 mL), to which FITC (28.0 mg, 0.072 mmol) was added. The solution was stirred for 12 h at room temperature and protected from light. Meanwhile, 200.0 mg of mPEG-*b*-(PPLG-*g*-MSA) lyophilized powder was weighed into a glass vial, and dissolved in DMSO (5.0 mL), followed by addition of EDC · HCl (20.6 mg, 0.108 mmol) and NHS (8.3 mg, 0.072 mmol). After stirred overnight at room temperature with protection from light, the amine-modified FITC was covalently linked to mPEG-*b*-(PPLG-*g*-MSA) with activated carboxyl group by adding FITC solution dropwise to mPEG-*b*-(PPLG-*g*-MSA) solution. The mixture was stirred for another 24 h at room temperature, and then purified by dialysis against deionized water for 48 h. A light yellow powder was obtained after lyophilization. DOX · HCl was loaded into FITC-labeled mPEG-*b*-(PPLG-*g*-MSA) by the same procedure described above.

© 2013 WILEY-VCH Verlag GmbH & Co. KGaA, Weinheim

2.6. In vitro Release of DOX · HCl

To determine the release profiles of DOX · HCl, the weighed freeze-dried mPEG-*b*-(PPLG-*g*-MSA)-DOX · HCl powder was suspended in 10 mL of release medium and transferred into a dialysis bag (MWCO 3500 Da). The release experiment was initiated by placing the end-sealed dialysis bag into 40 mL of release medium at 37 °C with constant shaking. At selected time intervals, 3 mL of release media was taken out and replenished with an equal volume of fresh media. The amount of DOX·HCl released was determined using UV-Vis spectrometer at 480 nm.

2.7. Cell Cultures

The human lung carcinoma (A549) cells and human cervical carcinoma (HeLa) cells were cultured at 37 °C in a 5% CO_2 atmosphere in Dulbecco's modified Eagle's medium (DMEM, Gibco) supplemented with 10% fetal bovine serum (FBS), penicillin (50 U mL^{-1}) and streptomycin (50 U mL^{-1}).

2.8. Confocal Laser Scanning Microscopy (CLSM) Observation

The cellular uptake and intracellular release behaviors of mPEG-*b*-(PPLG-*g*-MSA)-DOX · HCl were determined by CLSM toward A549 cells. The cells were seeded on the coverslip in 6-well plates with a density of 1×10^5 cells per well in 2 mL of DMEM and cultured for 24 h, and then the original medium was replaced with free DOX · HCl and mPEG-*b*-(PPLG-*g*-MSA)-DOX · HCl (at a final DOX · HCl concentration of 5 mg L^{-1}) containing DMEM. After 1 and 3 h incubation, the cells were washed and fixed with 4% formaldehyde for 20 min at room temperature. The cells were counterstained with DAPI for cell nucleus and Alexa Fluor 488 phalloidin (Invitrogen, Carlsbad, CA, USA) for F-actin following the manufacturer's instructions. The cellular localization was visualized under a laser scanning confocal microscope (Olympus FluoView 1000).

The cellular internalization and the accumulation of FITC-labeled mPEG-*b*-(PPLG-*g*-MSA)-DOX · HCl were monitored by CLSM (Olympus FluoView 1000). Briefly, the cells were seeded on the coverslip in 6-well plates with a density of 1×10^5 cells per well in 2 mL of DMEM and cultured for 24 h, and then the original medium was replaced with FITC-labeled mPEG-*b*-(PPLG-*g*-MSA)-DOX · HCl (at a final DOX · HCl concentration of 5 mg L^{-1}) containing DMEM. After 1 and 3 h incubation at 4 and 37 °C, the cells were washed and fixed with 4% formaldehyde for 20 min at room temperature, and the cell nuclei were stained with DAPI. Finally, the cells were monitored by CLSM.

2.9. Cellular Uptake Measured by Flow Cytometry

A549 or HeLa cells were seeded in 6-well plates with a density of 2×10^5 cells per well in 2 mL of DMEM and incubated for 24 h, and then the original medium was replaced with free DOX · HCl and mPEG-*b*-(PPLG-*g*-MSA)-DOX · HCl (at a final DOX · HCl concentration of 5 mg L^{-1}) containing DMEM. The cells were incubated for 1 and 3 h at 37 °C, and then washed three times with phosphate buffered saline (PBS). The harvested cells were suspended in PBS and centrifuged at 1000 rpm for 5 min at 4 °C. The supernatants were discarded and the cells were washed with PBS to remove the background fluorescence in the medium. After two cycles of washing and centrifugation, cells were resuspended with 500 μL of PBS, and flow cytometry was done using a BD FACSCalibur flow cytometer from BD Biosciences.

2.10. Cytotoxicity Assay

The cytotoxicities of mPEG-*b*-(PPLG-*g*-MSA), free DOX · HCl and mPEG-*b*-(PPLG-*g*-MSA)-DOX · HCl were evaluated by MTT assay. The cells were seeded in 96-well plates (1×10^4 cells per well) in 100 μL of DMEM medium and incubated at 37 °C in a 5% CO_2 atmosphere for 24 h. The culture medium was replaced with 200 μL of fresh medium containing mPEG-*b*-(PPLG-*g*-MSA), free DOX · HCl or mPEG-*b*-(PPLG-*g*-MSA)-DOX · HCl. The cells were subjected to MTT assay after being incubated for another 24 h. The absorbency of the solution was measured on a Bio-Rad 680 microplate reader at 490 nm. The relative cell viability was determined by comparing the absorbance at 490 nm with control wells containing only cell culture medium. Data are presented as means ± SD ($n = 6$).

2.11. Cell Apoptosis Analysis

Annexin V-FITC apoptosis detection kit (Keygen Biotech, China) was used to quantify the apoptotic and necrotic cells by a standard fluorescent activated cell sorting (FACS) assay. A549 cells were double stained with Annexin V and propidium iodide (PI), and then subject to flow cytometry. A549 cells were seeded in 6-well plates with a density of 2×10^5 cells per well in 2.0 mL of DMEM and incubated for 24 h, and then the original medium was removed and replaced with mPEG-*b*-(PPLG-*g*-MSA), free DOX · HCl and mPEG-*b*-(PPLG-*g*-MSA)-DOX · HCl containing DMEM (at a final DOX · HCl concentration of 5.0 mg · L^{-1}). After 24 h incubation, the cells were digested with EDTA-free trypsin, washed twice with cold PBS, and resuspended in binding buffer. Then, the cells were stained with 5.0 μL of Annexin V-FITC solution and 5.0 μL of PI solution for 15 min at room temperature in the dark. At the end of incubation, 400.0 μL of binding buffer was added, and the cells were analyzed immediately using flow cytometry.

2.12. Hemolysis Assay

Hemolytic activity of mPEG-*b*-(PPLG-*g*-MSA), free DOX · HCl and mPEG-*b*-(PPLG-*g*-MSA)-DOX · HCl were evaluated according to the previous protocol with minor modification.[24] Briefly, freshly rabbit blood obtained from the Laboratory Animal Center of Jilin University was diluted by physiological saline, and then red blood cells (RBCs) were isolated from serum by centrifugation. After carefully wash and dilution, RBC suspension was added to mPEG-*b*-(PPLG-*g*-MSA), free DOX · HCl and mPEG-*b*-(PPLG-*g*-MSA)-DOX · HCl solution at systematically varied concentrations and mixed by vortex, then incubated at 37 °C in a thermostatic water bath for 1.5 h. PBS and Triton X-100 (10 g · L^{-1}), a surfactant known to lyse RBCs, were used as negative and positive controls, respectively. Then, RBCs were centrifuged at 3 000 rpm for 10 min and 100 μL of supernatant of each sample was transferred to a 96-well plate. Free hemoglobin in the supernatant was measured with a Bio-Rad 680 microplate reader at 540 nm. The HR of RBCs was calculated using the following formula: hemolysis (%) = $(A_{sample} - A_{negative\ control})$/

© 2013 WILEY-VCH Verlag GmbH & Co. KGaA, Weinheim

$(A_{positive\ control} - A_{negative\ control}) \times 100$, where A_{sample}, $A_{negative\ control}$, and $A_{positive\ control}$ were denoted as the absorbencies of samples, negative and positive controls, respectively. All hemolysis experiments were carried out in triplicates.

2.13. Ex vivo DOX Fluorescence Imaging

The mPEG-*b*-(PPLG-*g*-MSA)-DOX · HCl and free DOX · HCl were injected into mice bearing A549 tumor via lateral tail vein (5 mg kg^{-1} on a DOX · HCl basis). The mice were sacrificed 2 and 24 h post-injection. The tumor and major organs (heart, liver, spleen, lung, and kidney) were excised, followed by washing the surface with physiological saline three times for ex vivo imaging of DOX · HCl fluorescence using the Maestro in vivo Imaging System (Cambridge Research & Instrumentation, Inc., USA).

2.14. In vivo Antitumor Efficiency

Male Balb/C nude mice were obtained from SLRC Laboratory Animal Company (Shanghai, China), and used at 6 weeks of age. All animals received care in compliance with the guidelines outlined in the Guide for the Care and Use of Laboratory Animals and all procedures were approved by the Animal Care and Use Committee of Jilin University.

A human non-small cell lung cancer (NSCLC) xenograft tumor model was generated by subcutaneous injection of A549 cells (1.5×10^6) in the right flank of each mouse. When the tumor volume was approximately 50 mm^3, mice were randomly divided into five groups. Animals were treated with PBS, free DOX · HCl (2 mg kg^{-1}), free DOX · HCl (4 mg kg^{-1}), mPEG-*b*-(PPLG-*g*-MSA)-DOX · HCl (2 mg kg^{-1} on a DOX · HCl basis) and mPEG-*b*-(PPLG-*g*-MSA)-DOX · HCl (4 mg kg^{-1} on a DOX · HCl basis) by intravenous injection on days 0, 3, 7, and 10. The tumor size was measured using vernier calipers, and the tumor volume (mm^3) was calculated using $V = ab^2/2$, where a and b were the longest and shortest diameter of the tumors. The body weight was measured simultaneously as an indicator of systemic toxicity.

2.15. Histological and Immunohistochemical Analyses

The mice were sacrificed (1 week after the last treatment) and tumors were collected, fixed in 4% PBS buffered paraformaldehyde overnight, and then embedded in paraffin. The paraffin-embedded tumors were cut at 5 μm thickness, and stained with hematoxylin and eosin to assess histological alterations by microscope (Nikon TE2000U).

Immunohistochemistry was performed as described previously.[25] Rabbit monoclonal primary antibody for cleaved PARP (Abcam, Cambridge, MA, USA) and PV-6000 two-step immunohistochemistry kit (polymer detection system for immuno-histological staining; Zhongshan Goldbridge Biotechnology, Beijing, China) were used in this study.

2.16. In Situ Terminal Deoxynucleotidyl Transferase–Mediated Deoxyuridine Triphosphate Nick End Labeling (TUNEL) Assay

TUNEL assay was performed using a FragELTM DNA fragment detection kit (colorimetric-TdT Enzyme method) according to the manufacturer's protocol (EMD chemicals Inc, Darmstadt, Germany) with minor modification. In brief, hematoxylin was used as counterstain to replace methyl green.

2.17. Statistical Analysis

All experiments were performed at least three times and expressed as means ± SD. Data were analyzed for statistical significance using Student's test. $p < 0.05$ was considered statistically significant, and $p < 0.01$ was considered highly significant.

3. Results and Discussion

3.1. Synthesis of mPEG-*b*-(PPLG-*g*-MSA)

The MSA-functionalized biodegradable mPEG-*b*-PPLG copolypeptides were developed as DOX · HCl delivery carriers. mPEG-*b*-(PPLG-*g*-MSA) was synthesized by combining ROP of a clickable monomer of PLG-NCA and subsequent thiol-yne photochemistry (Scheme 1). The ^{1}H NMR spectrum of mPEG-*b*-PPLG recorded in CF_3COOD is displayed in

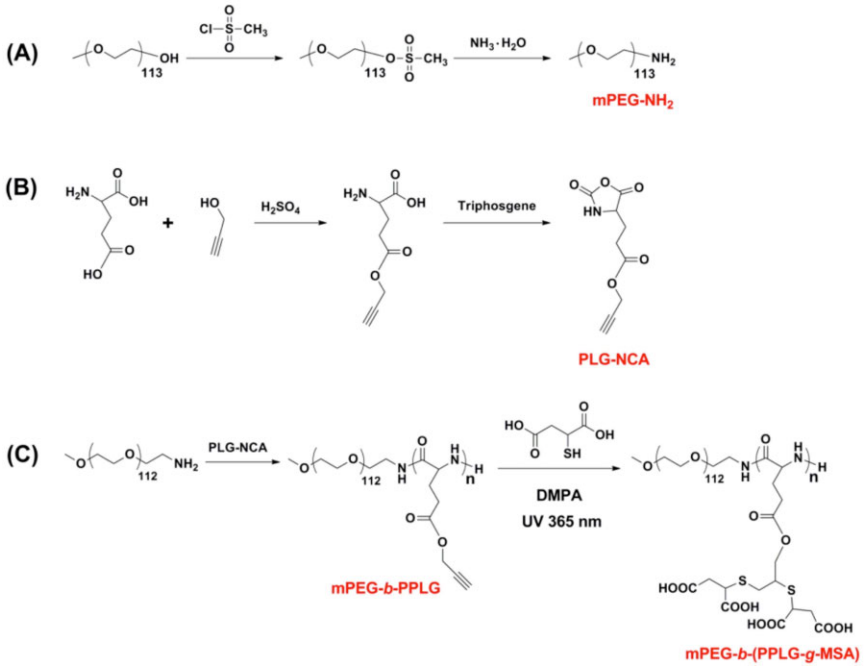

Scheme 1. Synthetic routes for the preparation of A) mPEG-NH_2, B) PLG-NCA, and C) mPEG-*b*-(PPLG-*g*-MSA).

© 2013 WILEY-VCH Verlag GmbH & Co. KGaA, Weinheim

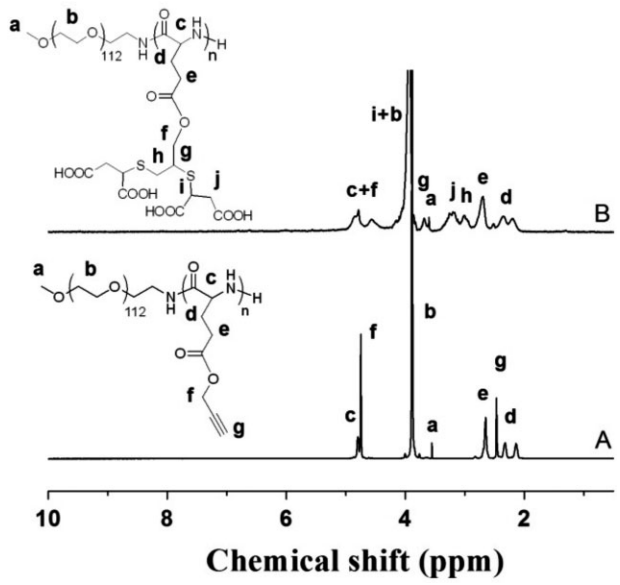

Figure 1. ^{1}H NMR spectra of A) mPEG-*b*-PPLG and B) mPEG-*b*-(PPLG-*g*-MSA) in CF_3COOD.

Figure 1A with the relevant signals labeled. The actual degree of polymerization ($\overline{DP}$) of PPLG block was determined to be 25 by comparing integration areas of peak *b* (–CH_2CH_2O–, 4H, mPEG block) in the range of 3.97–3.78 ppm with that of peak *e* (—COCH_2—, 2H, PPLG block) in the range of 2.76–2.55 ppm. The FT-IR spectrum of mPEG-*b*-PPLG (Figure 2A) clearly reveals the presence of absorbance peak at 2127 cm^{-1} characteristic of alkynyl moieties. The GPC trace (Figure S1, Supporting Information) was monomodal and quite symmetric, revealing the number average molecule weight ($\overline{M}_n$) of 18.6×10^3 $gmol^{-1}$ and polydispersity index (PDI, $\overline{M}_w/\overline{M}_n$) of 1.30. In comparison with that of

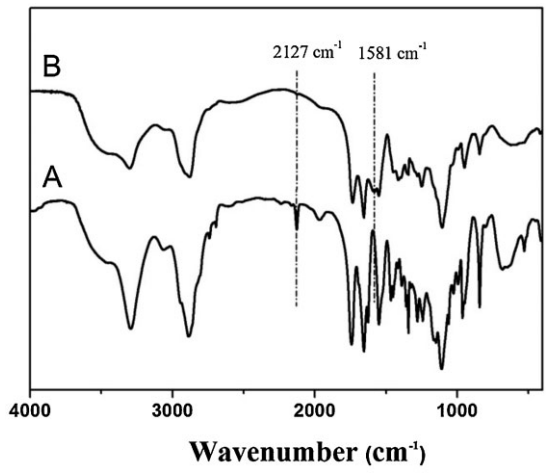

Figure 2. FT-IR spectra obtained for A) mPEG-*b*-PPLG and B) mPEG-*b*-(PPLG-*g*-MSA).

mPEG-NH_2, GPC trace of mPEG-*b*-PPLG exhibited a clear shift to the higher $\overline{M}_n$ region, indicating successful block copolymerization.

As reported by Neoh and co-workers, and Stenzel and co-workers, the radical-initiated thiol-yne click chemistry postpolymerization modification has been applied to synthesize copolymers with high efficiency via clicking of MSA to the alkyne side chains of non-degradable radical polymers.[26] However, there were few reports on clicking of MSA to the side chains of biodegradable polymer. In our study, thiol functionalized MSA was grafted onto the polypeptide backbone under UV irradiation in the presence of DMPA. The graft ratio of MSA was determined to be 69%, based on the integral ratio of peak *j* and *h* to peak *e* in the ^{1}H NMR spectrum of mPEG-*b*-(PPLG-*g*-MSA) (Figure 1B). The FT-IR spectrum (Figure 2B) shows the disappearance of alkyne characteristic absorbance at 2127 cm^{-1} and appearance of carboxylate band at 1581 cm^{-1} from MSA moieties. GPC analyses (Figure S2B, Supporting Information) indicate a narrow molecular weight distribution with a PDI of 1.13 for the side-chain functionalized block polypeptide. A combination of ^{1}H NMR, FT-IR, and GPC verified the successful synthesis of mPEG-*b*-(PPLG-*g*-MSA) with high purity and narrow polydispersity.

3.2. Preparation of the DOX · HCl-loaded mPEG-*b*-(PPLG-*g*-MSA) Complexes

DOX · HCl is a positively charged amphiphilic drug, containing protonable amino group in the sugar moiety. Carboxyl group rich polymers, such as poly(glutamic acid),[21e] poly(acrylic acid),[21b] and poly(methacrylic acid)[21c] have been reported to generate polymer-DOX · HCl complexes. However, polymers with bidentate dicarboxylic ligands had not previously been reported for DOX · HCl encapsulation. The side-chain functionalized polymers with neighboring carboxyl groups might promote the stability of counterion complex in solution, resulting in structurally better defined drug-loaded vehicle. In the present study, a polymer with bidentate dicarboxylic groups was synthesized via thiol-yne "click" reaction between the well-defined mPEG-*b*-PPLG precursor and thiol functionalized MSA. DOX · HCl loading was performed by incubating the click product mPEG-*b*-(PPLG-*g*-MSA) and DOX · HCl in aqueous medium below its pK_a value (Scheme 2), then dialyzing the polymer/drug solution to remove unloaded drug, and lyophilizing for long-term storage. The DLC and DLE of mPEG-*b*-(PPLG-*g*-MSA)-DOX · HCl were calculated to be 16.5 and 99.0 wt%, respectively. It was inferred that both the electrostatic interaction between cationic DOX · HCl and anionic carriers, and the hydrophobic stack between DOX · HCl and carriers or DOX · HCl molecule itself, were contributed to the effective drug encapsulation.[21e][21f][27] Polymersomes with uniform size

© 2013 WILEY-VCH Verlag GmbH & Co. KGaA, Weinheim

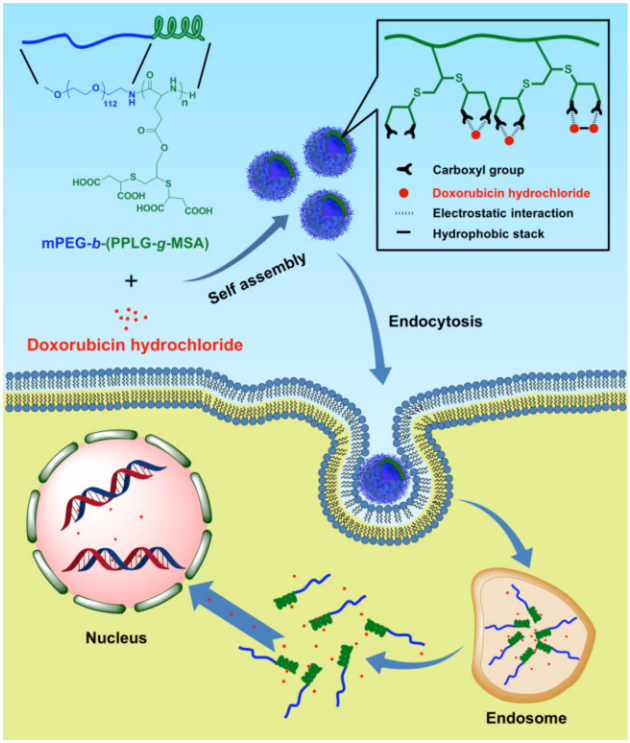

Scheme 2. Schematic illustration of drug loading, endocytosis and intracellular drug release of the pH-responsive amphiphile polymersome.

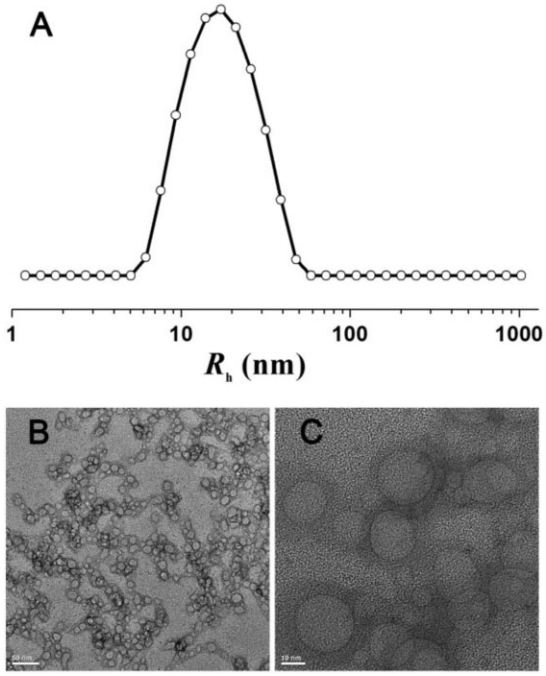

Figure 3. A) Hydrodynamic radius distribution and B,C) morphology of mPEG-*b*-(PPLG-*g*-MSA)-DOX · HCl in aqueous solution as determined by DLS and TEM.

(Figure 3) were obtained when the lyophilized powder of mPEG-*b*-(PPLG-*g*-MSA)-DOX · HCl was redissolved in water. The similar vesicle structure was obtained in the work of Sanson et al.,[21e] where DOX · HCl was loaded into poly (trimethylene carbonate)-*b*-poly(L-glutamic acid). TEM micrograph showed that mPEG-*b*-(PPLG-*g*-MSA)-DOX · HCl took clear vesicular morphology with the respective average diameter around 20 nm (Figure 3B). The hydrodynamic diameter (D_h) measured by DLS was 34 ± 5 nm, which might be an optimal size for the tumor targeting by the enhanced permeability and retention (EPR) effect.[28] The smaller size from TEM observations should be due to the dehydration of the DOX · HCl-loaded polymersomes in the TEM sample preparation process.[19,29] The mPEG-*b*-(PPLG-*g*-MSA)-DOX · HCl exhibited a negative surface charge (-39.1 ± 3.5 mV), indicating good dispersion stability,[30] which will also minimize the undesirable rapid elimination of DOX · HCl-loaded polymersomes from the blood circulation, and facilitate their accumulation at the tumor sites.[31]

3.3. In vitro Release of DOX · HCl

The in vitro release profiles of mPEG-*b*-(PPLG-*g*-MSA)-DOX · HCl were evaluated at pH 7.4 and 5.5 by dialysis method. As shown in Figure 4, the release profile of DOX · HCl from DOX · HCl-loaded polymersomes displayed a biphasic pattern that was characterized by a first rapid release followed by a slower and sustained release. There was approximately 62.8% release at pH 5.5 after a 60 h incubation period, while 27.2% release at pH 7.4. Drug release under physiological conditions (pH 7.4) was significantly lower than that under acidic conditions (pH 5.5), which might be attributed to a significant reduction in the ionization degree of MSA moieties, resulting in

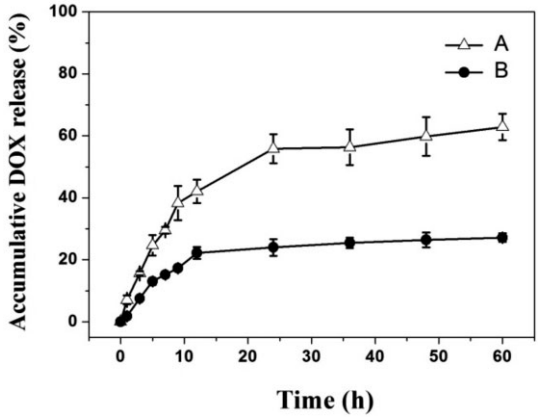

Figure 4. Time- and pH-dependent DOX · HCl release profiles of DOX · HCl-loaded polymersomes in A) PBS at pH 5.5 and B) PBS at pH 7.4. The data presented are means ± SD ($n = 3$).

© 2013 WILEY-VCH Verlag GmbH & Co. KGaA, Weinheim

extensive disruption of their electrostatic interactions with DOX · HCl.[21f] In addition, increased hydrophilicity of DOX · HCl in acid condition also result in a rapid release of DOX · HCl.[21e] Such a pH-triggered release behavior of DOX · HCl showed great potential in drug delivery for the anti-proliferative effect, due to the release of DOX · HCl in cells while limiting its release in blood circulation (Scheme 2).[25b]

3.4. Intracellular Drug Delivery

To investigate the cellular internalization and intracellular release of DOX · HCl, the DOX · HCl-loaded polymersomes were incubated with A549 cells for 1 and 3 h at 37 °C. The cells were then observed by CLSM. The cellular nuclei and cytoskeleton of A549 cells were selectively stained with DAPI (blue) and Alexa Fluor 488 (green), respectively. Red fluorescence imaging was performed to visualize the released DOX · HCl (Figure 5). After 1 h incubation with free DOX · HCl and mPEG-*b*-(PPLG-*g*-MSA)-DOX · HCl, the DOX · HCl fluorescence was both found to be aggregated in the cytosol and nuclei in both samples, whereas the DOX · HCl fluorescence intensity of mPEG-*b*-(PPLG-*g*-MSA)-DOX · HCl observed in nuclei was slightly weaker than that of free DOX · HCl. When the incubation period was increased to 3 h, DOX · HCl was found mainly located in the cell nuclei and perinuclear region in both cases, but slightly stronger emission intensities of the cell nuclei had been obtained for free DOX · HCl. It should be noted that stronger DOX · HCl fluorescence was observed in cells following incubation with free DOX · HCl for 1 and 3 h, compared with the mPEG-*b*-(PPLG-*g*-MSA)-DOX · HCl group. This phenomenon had also been observed by other groups before, which could be explained by the slightly slower cellular uptake of DOX · HCl-loaded polymersomes that were shielded by a dense layer of PEG shells and delayed drug release from the polymersomes.[32] For further confirmation, the cellular uptake of DOX · HCl and mPEG-*b*-(PPLG-*g*-MSA)-DOX · HCl into the A549 cells were analyzed using fluorescence-activated flow cytometry (Figure 6), and the consistent results were acquired. Similar results were obtained for HeLa cells (Figure S4, Supporting Information).

Endocytosis, a general entry mechanism for macromolecules, is an ATP (adenosine triphosphate)-dependent process, which is attenuated down at low temperatures.[33] In order to assess whether the DOX · HCl-loaded polymersonmes enter cells via endocytosis, we incubated cells with FITC-labeled mPEG-*b*-(PPLG-*g*-MSA)-DOX · HCl and compared the fluorescence accumulation to cells at 4 and 37 °C via CLSM analysis. Incubation of A549 cells with FITC-labeled polymersomes at 37 °C resulted in a time-dependent internalization. In contrast, the treatment at lower temperature which interfering with endocytosis resulted in a decrease of cellular uptake of FITC-labeled polymersomes as shown in confocal microscope images (Figure S5, Supporting Information), suggesting that the DOX · HCl-loaded polymersonmes were taken up by A549 cells via endocytosis.

3.5. In vitro Cytotoxicity and Apoptotic Activity

The biocompatibility studies using A549 and HeLa cells revealed that mPEG-*b*-(PPLG-*g*-MSA) was non-toxic up to

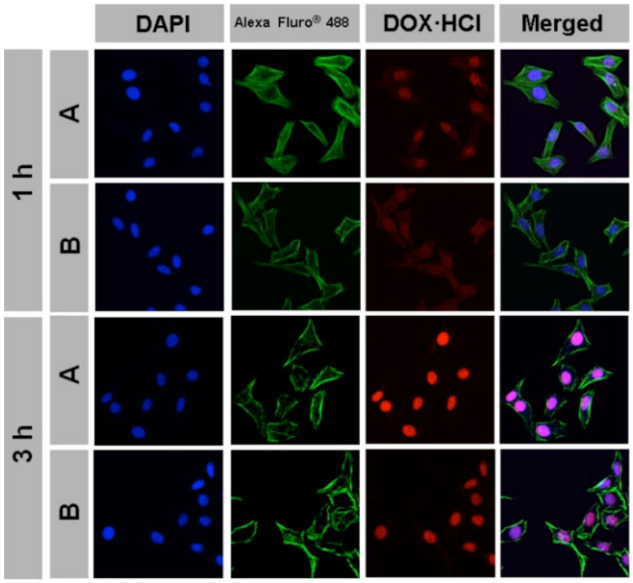

Figure 5. Cellular uptake of A) free DOX · HCl and B) mPEG-*b*-(PPLG-*g*-MSA)-DOX · HCl after incubation with A549 cells for 1 and 3 h.

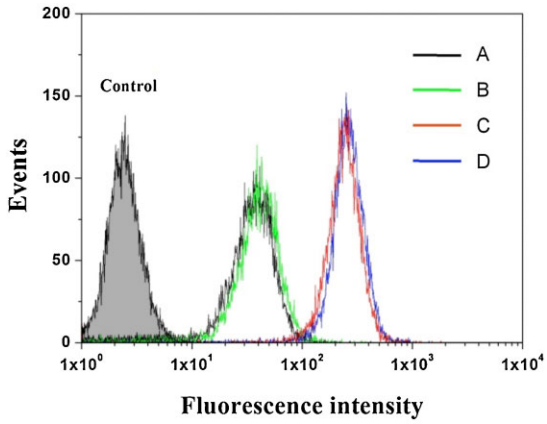

Figure 6. The FACS analysis of cellular uptake of free DOX · HCl and mPEG-*b*-(PPLG-*g*-MSA)-DOX · HCl after incubation with A549 cells for 1 and 3 h. A) mPEG-*b*-(PPLG-*g*-MSA)-DOX · HCl, 1 h; B) free DOX · HCl, 1 h; C) mPEG-*b*-(PPLG-*g*-MSA)-DOX · HCl, 3 h; and D) free DOX · HCl, 3 h.

© 2013 WILEY-VCH Verlag GmbH & Co. KGaA, Weinheim

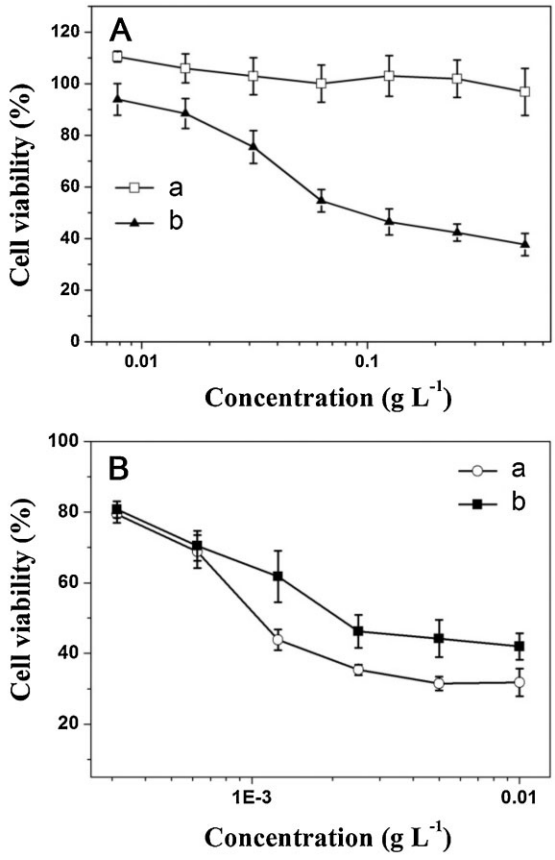

Figure 7. A) In vitro cytotoxicities of a) mPEG-*b*-(PPLG-*g*-MSA) to A549 cells with b) PEI25K as positive control; B) cytotoxicities of a) free DOX · HCl and b) mPEG-*b*-(PPLG-*g*-MSA)-DOX · HCl to A549 cells.

the highest testing concentration of 500 mg L^{-1} (Figure 7A and Figure S3, Supporting Information), whereas there were much fewer live cells left after treatment with PEI25K at the same concentration (especially at the high concentration), indicating its excellent biocompatibility. At an equivalent drug concentration, DOX · HCl-loaded polymersomes revealed a slightly lower antitumor activity as compared to free DOX · HCl (Figure 7B), which agreed well with the intracellular DOX · HCl release observations (Figure 5). It was due to free DOX · HCl of an amphipathic small molecule that can easily cross the cell membrane, while the DOX · HCl release from the polymersomes was accelerated within the acidic intracellular endosome/lysosome, thus resulting in the higher cytotoxic efficiency than mPEG-*b*-(PPLG-*g*-MSA)-DOX · HCl. However, for in vivo applications, it is unlikely that such a high concentration of free DOX · HCl would be present for such a long treatment time.[34] On the other hand, DOX · HCl-loaded polymersome formulation with long circulating property may facilitate its passive accumulation at tumor tissue via EPR effect.[35]

Further, the death mechanisms of A549 cells treated with free DOX · HCl and mPEG-*b*-(PPLG-*g*-MSA)-DOX · HCl were evaluated by flow cytometry. Cells were double stained for viability (negative for PI) and apoptosis (positive for Annexin V-FITC). As shown in Figure 8, mPEG-*b*-(PPLG-*g*-MSA)-DOX · HCl obviously induced A549 cell apoptosis, whereas mPEG-*b*-(PPLG-*g*-MSA) did not. Free DOX · HCl at 5 mg L^{-1} killed 99% cells via necrosis and apoptosis. However, mPEG-*b*-(PPLG-*g*-MSA)-DOX · HCl at an equivalent drug concentration resulted in limited cytotoxic effects on A549 cells (Figure 8). Taking into account the in vitro drug release and intracellular drug delivery results, this can be ascribed to the comparably slower internalization and drug release from the carrier.

3.6. Hemolysis

The application of the vesicular formulations in the pharmaceutical field counts on several aspects including safety, DLE, and stability. It is necessary to guarantee the blood compatibility of the drug-loaded nanocomposite, because it will be finally injected intravenously into blood vessels. In this study, a hemolysis assay was carried out

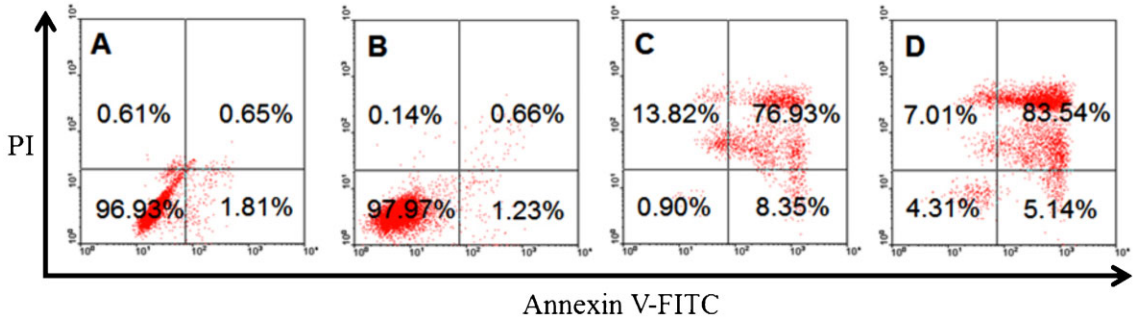

Figure 8. Apoptotic cell populations determined by flow cytometric analysis with Annexin V-FITC and PI staining after incubating A549 cells in DMEM media, with A) media alone; B) mPEG-*b*-(PPLG-*g*-MSA); C) free DOX · HCl; and D) mPEG-*b*-(PPLG-*g*-MSA)-DOX · HCl. The lower-left and upper-left quadrants in each panel indicate the populations of normal cells and necrotic cells, respectively, whereas the lower-right and upper-right quadrants in each panel indicate the populations of early and late apoptotic cells, respectively.

© 2013 WILEY-VCH Verlag GmbH & Co. KGaA, Weinheim

based on the previous report.[3b][36] As shown in the Figure S6A (Supporting Information), mPEG-*b*-(PPLG-*g*-MSA) showed negligible hemolysis toxicity (≈0%) to RBCs even at the highest polymer concentration of 5 g L^{-1}, demonstrating the excellent blood compatibility of mPEG-*b*-(PPLG-*g*-MSA). The DOX · HCl-loaded polymersomes significantly decreased the hemolysis of the RBCs compared to free DOX · HCl (Figure S6, Supporting Information). The depressed hemolytic activity should be originated from the outmost PEG shell serving as a protective layer, and the negatively charged surface.[37] These results indicated that DOX · HCl-loaded polymersomes were hemocompatible, allowing the potential application as drug delivery vehicles.

3.7. Ex vivo DOX · HCl Fluorescence Imaging

For biodistribution studies, imaging of the isolated visceral organs (heart, liver, spleen, lung, and kidney) and tumors at 2 and 24 h post-injection were carried out in nude mice bearing A549 tumor, and the results are shown in Figure 9. At 2 h post-injection, liver and kidney showed strong DOX · HCl fluorescence for free DOX · HCl group, suggesting that drug molecules as foreign bodies were mainly captured and metabolized by liver and kidney.[38] However, the fairly weaker fluorescence in both liver and kidney, and the stronger fluorescence in tumor for the injection of mPEG-*b*-(PPLG-*g*-MSA)-DOX · HCl were observed, indicating that the DOX · HCl-loaded polymersomes were able to alter the biodistribution of the drug and contribute to reduce the drug's systemic toxicity. This result also suggests that the maximum tolerated dose (MTD) of DOX · HCl can be increased through mPEG-*b*-(PPLG-*g*-MSA) polymersome-mediated delivery. At 24 h post-injection, DOX fluorescence

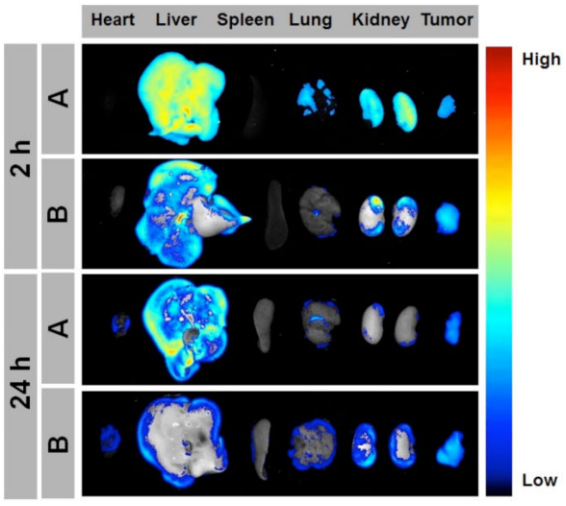

Figure 9. Ex vivo DOX · HCl fluorescence images showing the drug bio-distribution of A) free DOX · HCl and B) mPEG-*b*-(PPLG-*g*-MSA)-DOX · HCl in nude mice bearing A549 tumor at 2 and 24 h post-injection.

in tumor was slightly weakened as detected in ex vivo imaging, and meanwhile liver and kidney showed even much weaker fluorescence for both free DOX · HCl and mPEG-*b*-(PPLG-*g*-MSA)-DOX · HCl formulations. A stronger fluorescence signal was also found in tumor administered by mPEG-*b*-(PPLG-*g*-MSA)-DOX · HCl compared with that of free DOX · HCl, which could contribute to increase the cancer therapy efficiency by EPR effect.[39]

3.8. In vivo Anticancer Efficacy

Based on the promising results from in vitro experiments, the in vivo antitumor efficacy was further investigated on Balb-c/nude mice bearing human lung tumors (A549). The treatments were done by intravenously injecting PBS, free DOX · HCl (2 and 4 mg kg^{-1}), the DOX-loaded mPEG-*b*-(PPLG-*g*-MSA) polymersomes (2 and 4 mg kg^{-1} DOX · HCl eq.), respectively, into tumor-bearing mice. All the mice were alive during the experimental period. As shown in Figure 10A, compared with the control (treatment with PBS), the tumor growth was effectively inhibited in all the groups treated with free DOX · HCl and the mPEG-*b*-(PPLG-*g*-MSA)-DOX · HCl formulations. Administration of free DOX · HCl was effective in tumor regression to some extent, but the free DOX · HCl did not demonstrate comparable efficacy to the mPEG-*b*-(PPLG-*g*-MSA)-DOX · HCl. After administration for 17 d, the average tumor volumes of free DOX · HCl (2 mg kg^{-1}), free DOX · HCl (4 mg · kg^{-1}), mPEG-*b*-(PPLG-*g*-MSA)-DOX · HCl (2 mg kg^{-1} DOX · HCl eq.), and mPEG-*b*-(PPLG-*g*-MSA)-DOX · HCl (4 mg · kg^{-1} DOX · HCl eq.) were 23.1, 14.2, 13.4, and 5.4% of that in the control group, respectively ($p < 0.001$), indicating enhanced efficiency of DOX · HCl-loaded polymersome formulations and a dose-dependent antitumor activity. On the other hand, the average tumor volume of the group b (free DOX · HCl, 2 mg kg^{-1}) was about 1.7-fold ($p < 0.01$) and 4.3-fold ($p < 0.001$), compared to that of the group d (mPEG-*b*-(PPLG-*g*-MSA)-DOX · HCl, 2 mg kg^{-1} DOX · HCl eq.) and group e (mPEG-*b*-(PPLG-*g*-MSA)-DOX · HCl, 4 mg · kg^{-1} DOX · HCl eq.), respectively. The comparison between group d (mPEG-*b*-(PPLG-*g*-MSA)-DOX · HCl, 2 mg kg^{-1} DOX · HCl eq.) and e (mPEG-*b*-(PPLG-*g*-MSA)-DOX · HCl, 4 mg kg^{-1} DOX · HCl eq.) revealed the obvious dose dependence of the tumor inhibition ($p < 0.05$). These results indicated that the mPEG-*b*-(PPLG-*g*-MSA)-DOX · HCl inhibited tumor growth much more efficiently than free DOX · HCl formulation, and the group that received mPEG-*b*-(PPLG-*g*-MSA)-DOX · HCl at a dose of 4 mg kg^{-1} DOX · HCl showed the most effective antitumor efficacy among the testing groups. The enhanced tumor inhibition of the mPEG-*b*-(PPLG-*g*-MSA)-DOX · HCl might be explained by the enhanced accumulation of the DOX-loaded polymersomes at the tumor site. Furthermore, the effective encapsulation of DOX · HCl against leakage in the bloodstream and the facilitated intracellular release of

© 2013 WILEY-VCH Verlag GmbH & Co. KGaA, Weinheim

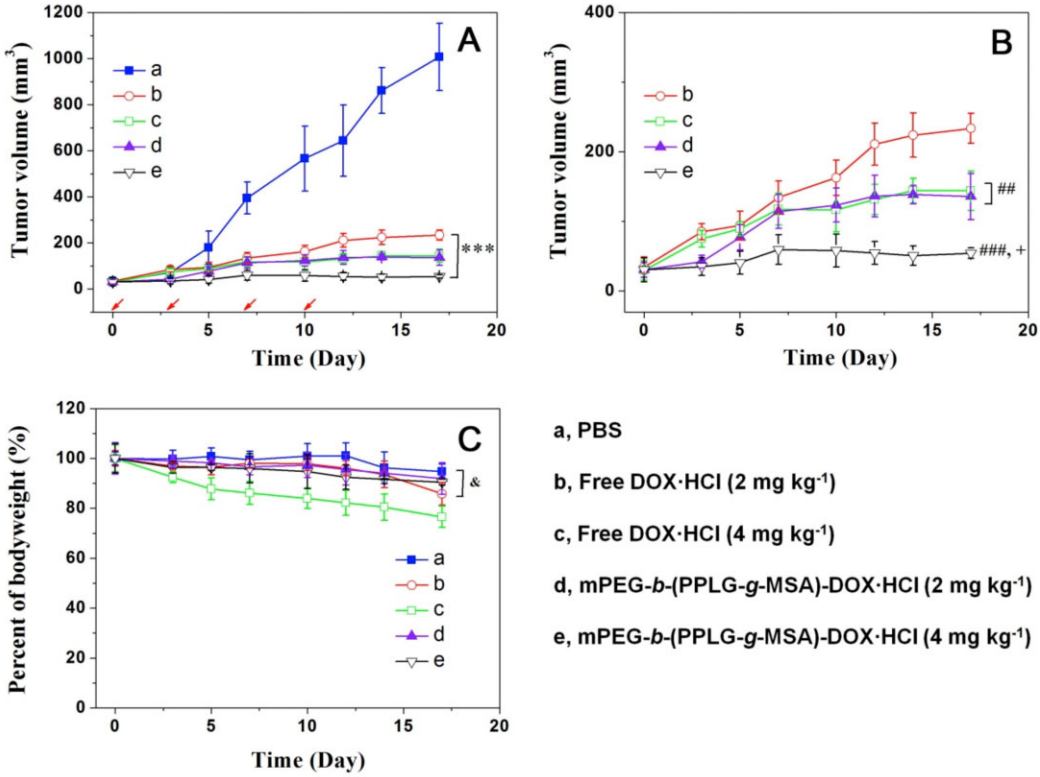

Figure 10. In vivo antitumor efficacy of various DOX · HCl formulations in the A549 tumor bearing mouse model. A) Tumor sizes of the mice as a function of time; B) amplificatory figure of tumor volume; C) body weight changes with the time of tumor-bearing mice. The arrows represent the day on which the intravenous tail vein injection was performed. $^{***}p < 0.001$ versus PBS group. $^{\#\#}p < 0.01$ and $^{\#\#\#}p < 0.001$ versus free DOX · HCl (2 mg kg^{-1}) group. $^{+}p < 0.05$ versus mPEG-*b*-(PPLG-*g*-MSA)-DOX · HCl (2 mg kg^{-1} DOX · HCl eq.) group. $^{\&}p < 0.01$ versus free DOX · HCl (4 mg kg^{-1}) group.

DOX · HCl might contribute to the observed enhanced antitumor efficacy.

Body weight loss is an important indicator to evaluate doxorubicin-induced toxicity. Figure 10C depicts the body weight of the mice during the test. Mice treated with free DOX ·HCl at a dose of 4 mg kg^{-1} exhibited a 24% decrease of body weight within 17 d, and appeared to be weak after treatment. Evident dose dependent systemic toxicity could be found, when group b (free DOX · HCl, 2 mg kg^{-1}) and c (free DOX · HCl, 4 mg kg^{-1}) were compared. In all other groups, the lack of significant change in body weight during the 17-day observation period confirmed the lower systemic toxicity.

These results indicate that mPEG-*b*-(PPLG-*g*-MSA)-DOX · HCl was an effective and safe enough drug formulation for the xenograft A549 cancer tumor model.

3.9. Histological and Immunohistochemical Analyses

To further evaluate the antitumor efficacy after treatment with various formulations, the tumors were dissected from mice and sectioned for pathology analyses.

As shown in Figure 11, the tumor cells with a large nucleus and a spherical or spindle shape were observed in the tumor tissue treated with PBS group, in which more chromatin and binucleolates were also observed. However, various degree of tissue necrosis were observed in the free DOX · HCl and mPEG-*b*-(PPLG-*g*-MSA)-DOX · HCl treated groups at 2 and 4 mg kg^{-1} doses. Chromatin was concentrated and distributed around the edge, and nuclei became pyknotic, fragmented or absence, especially for the mPEG-*b*-(PPLG-*g*-MSA)-DOX · HCl-treated tumor cells. The degree of pathological caryokinesis in the tumor was lowered and coagulation necrosis was enhanced as the DOX · HCl dose increased. The necrosis area in the mPEG-*b*-(PPLG-*g*-MSA)-DOX · HCl (4 mg kg^{-1} DOX · HCl eq.) group was the largest among the tested groups, while the free DOX · HCl and mPEG-*b*-(PPLG-*g*-MSA)-DOX · HCl (2 mg kg^{-1} DOX · HCl eq.) groups displayed a lower necrotic level. At the same DOX · HCl dose, the damage to tumor tissues treated with mPEG-*b*-(PPLG-*g*-MSA)-DOX · HCl was higher than that received free DOX · HCl.

Cell apoptosis in the tumors after treatment with various formulations were analyzed by the TUNEL assay. As shown

© 2013 WILEY-VCH Verlag GmbH & Co. KGaA, Weinheim

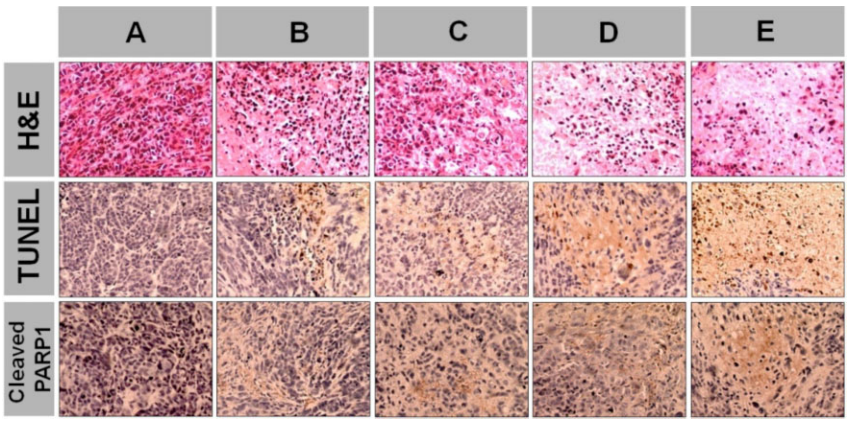

Figure 11. Ex vivo histological and immunohistochemical analyses of A549 tumor sections (17 d after the first treatment). A) PBS; B) free DOX · HCl (2 mg kg^{-1}); C) free DOX · HCl (4 mg kg^{-1}); D) mPEG-*b*-(PPLG-*g*-MSA)-DOX · HCl (2 mg kg^{-1} DOX · HCl eq.); and E) mPEG-*b*-(PPLG-*g*-MSA)-DOX · HCl (4 mg kg^{-1} DOX · HCl eq.). Nuclei were stained bluish violet, whereas extracellular matrix and cytoplasm were stained pink in H&E staining. Brown and blue stains indicated apoptotic and normal cells, respectively, in TUNEL analysis; brown and blue stains indicated cleaved PARP and nuclei, respectively, in immunohistochemical assay.

in Figure 11, little apoptosis was detected in tumor tissues treated by PBS. However, all the DOX·HCl formulations administered groups were detected obvious cell apoptosis. Consistent with the HE observation, treatment of DOX · HCl-loaded polymersomes increased apoptosis compared with free DOX·HCl at the same dose, whereas treatment of mPEG-*b*-(PPLG-*g*-MSA)-DOX·HCl at a dose of 4 mg kg^{-1} showed the highest degree of cell apoptosis in tumor tissue. This apoptosis was consistent with the results of the in vivo antitumor efficacy.

Poly-ADP-ribose polymerase (PARP), a nuclear enzyme that is catalytically activated by DNA strand interruptions, is one of the essential substrates cleaved by both caspase-3 and -7.[40] The presence of cleaved PARP1 is one of the most used diagnostic tools for the detection of apoptosis in many cell types.[25a] To further confirm the tumor apoptosis, the cleaved 25 kDa fragment of PARP1 was analyzed in the tumor sections by immunohistochemistry. The cleavage products were detected in the sections of tumor tissues treated with various DOX · HCl formulations. Intensive positive signals increased in the mPEG-*b*-(PPLG-*g*-MSA)-DOX · HCl (2 and 4 mg kg^{-1} DOX · HCl eq.) treated tumors compared with free DOX · HCl treated ones, indicating that more cells underwent apoptosis in these groups (Figure 11).

Together, these results demonstrated that mPEG-*b*-(PPLG-*g*-MSA)-DOX · HCl could efficiently deliver DOX · HCl to the NSCLC tumor, leading to reduced cell proliferation and increased apoptosis in vivo, which resulted in a persistent inhibition of tumor growth.

4. Conclusion

Side-chain functionalized mPEG-*b*-(PPLG-*g*-MSA) polypeptide with bidentate dicarboxylic groups was synthesized by combining ROP of a clickable monomer of PLG-NCA and subsequent thiol-yne photochemistry for DOX · HCl encapsulation. pH-responsive polymersomes with uniform size (≈20 nm) and high DLE (≈100%) were obtained from self-assembly of anionic polymer carrier and cationic DOX · HCl in aqueous medium. The excellent hemocompatibility, cytocompatibility, and drug loading capability of this copolypeptide rendered its potential for delivering bioactive substance via intravenous injection. CLSM and FACS studies confirmed that the FITC-labeled drug delivery polymersomes were taken up by A549 cells via endocytosis, with a slightly slower cellular internalization. This counterion complex could effectively protect the loaded DOX · HCl molecule and enhance DOX · HCl accumulation in tumors compared with that of free DOX · HCl. The in vivo study using a human NSCLC xenograft tumor model demonstrated lower toxicity and higher antitumor efficacy of mPEG-*b*-(PPLG-*g*-MSA)-DOX · HCl compared with free DOX · HCl at an equivalent drug dose. With convenient fabrication, favorable hemocompatibility and cytocompatibility, excellent drug loading and controlled release properties, the pH responsive polypeptide-based polymersomes held great potential for achieving an optimal therapeutic effect of the transported drugs in cancer treatment.

Acknowledgements: M.L. and S.L. contributed equally to this work. This research was financially supported by National Natural Science Foundation of China (Projects 51173184, 51273169, 21104076, 51233004, and 51021003), Ministry of Science and Technology of China (International Cooperation and Communication Program 2011DFR51090), Knowledge Innovation Program of the Chinese Academy of Sciences (Grant No. KJCX2-YW-H19).

Received: May 2, 2013; Revised: June 24, 2013; Published online: July 29, 2013; DOI: 10.1002/mabi.201300222

Keywords: drug delivery system; pH-responsive; polypeptide; self-assembly; thiol-yne photochemistry

[1] A. Lalatsa, A. G. Schatzlein, M. Mazza, B. H. L. Thi, I. F. Uchegbu, *J. Controlled Release* **2012**, *161*, 523.

© 2013 WILEY-VCH Verlag GmbH & Co. KGaA, Weinheim

[2] H. R. Kricheldorf, *Angew. Chem., Int. Ed.* **2006**, *45*, 5752.
[3] a) K. Wang, Y. Liu, W. J. Yi, C. Li, Y. Y. Li, R. X. Zhuo, X. Z. Zhang, *Soft Matter* **2013**, *9*, 692; b) W. Song, M. Li, Z. Tang, Q. Li, Y. Yang, H. Liu, T. Duan, H. Hong, X. Chen, *Macromol. Biosci.* **2012**, *12*, 1514; c) K. Wang, G. F. Luo, Y. Liu, C. Li, S. X. Cheng, R. X. Zhuo, X. Z. Zhang, *Polym. Chem.* **2012**, *3*, 1084.
[4] a) J. Yue, R. Wang, S. Liu, S. Wu, Z. Xie, Y. Huang, X. Jing, *Soft Matter* **2012**, *8*, 7426; b) J. X. Ding, X. L. Zhuang, C. S. Xiao, Y. L. Cheng, L. Zhao, C. L. He, Z. H. Tang, X. S. Chen, *J. Mater. Chem.* **2011**, *21*, 11383.
[5] a) C. S. Xiao, C. W. Zhao, P. He, Z. H. Tang, X. S. Chen, X. B. Jing, *Macromol. Rapid Commun.* **2010**, *31*, 991; b) Y. Cheng, C. He, C. Xiao, J. Ding, X. Zhuang, X. Chen, *Polym. Chem.* **2011**, *2*, 2627; c) J. X. Ding, C. S. Xiao, X. L. Zhuang, C. L. He, X. S. Chen, *Mater. Lett.* **2012**, *73*, 17.
[6] C. R. Becer, R. Hoogenboom, U. S. Schubert, *Angew. Chem., Int. Ed.* **2009**, *48*, 4900.
[7] H. Zhang, Y. Ma, X. L. Sun, *Chem. Commun.* **2009**, *21*, 3032.
[8] J. Sun, H. Schlaad, *Macromolecules* **2010**, *43*, 4445.
[9] S. B. Rahane, R. M. Hensarling, B. J. Sparks, C. M. Stafford, D. L. Patton, *J. Mater. Chem.* **2012**, *22*, 932.
[10] J. W. Chan, J. Shin, C. E. Hoyle, C. N. Bowman, A. B. Lowe, *Macromolecules* **2010**, *43*, 4937.
[11] Y. Huang, Y. Zeng, J. Yang, Z. Zeng, F. Zhu, X. Chen, *Chem. Commun.* **2011**, *47*, 7509.
[12] a) T. Negishi, F. Koizumi, H. Uchino, J. Kuroda, T. Kawaguchi, S. Naito, Y. Matsumura, *Br. J. Cancer* **2006**, *95*, 601; b) K. Kataoka, T. Matsumoto, M. Yokoyama, T. Okano, Y. Sakurai, S. Fukushima, K. Okamoto, G. S. Kwon, *J. Controlled Release* **2000**, *64*, 143; c) M. L. Adams, G. S. Kwon, *J. Controlled Release* **2003**, *87*, 23.
[13] a) D. Yang, X. Liu, X. Jiang, Y. Liu, W. Ying, H. Wang, H. Bai, W. D. Taylor, Y. Wang, J. P. Clamme, E. Co, P. Chivukula, K. Y. Tsang, Y. Jin, L. Yu, *J. Controlled Release* **2012**, *161*, 124; b) S. F. Yu, Z. Wang, G. L. Wu, Y. N. Wang, H. Gao, J. B. Ma, *Acta Polym. Sin.* **2012**, 427; c) F. Koizumi, M. Kitagawa, T. Negishi, T. Onda, S. Matsumoto, T. Hamaguchi, Y. Matsumura, *Cancer Res.* **2006**, *66*, 10048.
[14] Z. L. Tyrrell, Y. Shen, M. Radosz, *Prog. Polym. Sci.* **2010**, *35*, 1128.
[15] A. Lalatsa, A. G. Schatzlein, M. Mazza, T. B. Le, I. F. Uchegbu, *J. Controlled Release* **2012**, *161*, 523.
[16] a) A. Harada, K. Kataoka, *Macromolecules* **1998**, *31*, 288; b) A. Kano, K. Moriyama, T. Yamano, I. Nakamura, N. Shimada, A. Maruyama, *J. Controlled Release* **2011**, *149*, 2.
[17] N. Nishiyama, S. Okazaki, H. Cabral, M. Miyamoto, Y. Kato, Y. Sugiyama, K. Nishio, Y. Matsumura, K. Kataoka, *Cancer Res.* **2003**, *63*, 8977.
[18] H. T. Ta, C. R. Dass, I. Larson, P. F. M. Choong, D. E. Dunstan, *Biomaterials* **2009**, *30*, 3605.
[19] J. X. Ding, F. H. Shi, C. S. Xiao, L. Lin, L. Chen, C. L. He, X. L. Zhuang, X. S. Chen, *Polym. Chem.* **2011**, *2*, 2857.
[20] a) S. J. Lee, K. H. Min, H. J. Lee, A. N. Koo, H. P. Rim, B. J. Jeon, S. Y. Jeong, J. S. Heo, S. C. Lee, *Biomacromolecules* **2011**, *12*, 1224; b) Y. Xu, F. Meng, R. Cheng, Z. Zhong, *Macromol. Biosci.* **2009**, *9*, 1254.
[21] a) Y. Cheng, S. Yu, X. Zhen, X. Wang, W. Wu, X. Jiang, *ACS Appl. Mater. Interfaces* **2012**, *4*, 5325; b) Y. Du, W. Chen, M. Zheng, F. Meng, Z. Zhong, *Biomaterials* **2012**, *33*, 7291; c) N. V. Nukolova, H. S. Oberoi, S. M. Cohen, A. V. Kabanov, T. K. Bronich, *Biomaterials* **2011**, *32*, 5417; d) B. Manocha, A. Margaritis, *J. Nanomater.* **2010**, *2010*, 1; e) C. Sanson, C. Schatz, J. F. Le Meins, A. Soum, J. Thevenot, E. Garanger, S. Lecommandoux, *J. Controlled Release* **2010**, *147*, 428; f) W.-C. Huang, W.-H. Chiang, Y.-F. Huang, S.-C. Lin, Z.-F. Shih, C.-S. Chern, C.-S. Chiang, H.-C. Chiu, *J. Drug Target.* **2011**, *19*, 944.
[22] Y. G. Huang, Y. H. Zeng, J. W. Yang, Z. H. Zeng, F. M. Zhu, X. D. Chen, *Chem. Commun.* **2011**, *47*, 7509.
[23] M. J. Ernsting, W. L. Tang, N. MacCallum, S. D. Li, *Bioconjugate Chem.* **2011**, *22*, 2474.
[24] F. Shi, J. Ding, C. Xiao, X. Zhuang, C. He, L. Chen, X. Chen, *J. Mater. Chem.* **2012**, *22*, 14168.
[25] a) C. Fu, L. Lin, H. Shi, D. Zheng, W. Wang, S. Gao, Y. Zhao, H. Tian, X. Zhu, X. Chen, *Biomaterials* **2012**, *33*, 4589; b) J. Dai, S. Lin, D. Cheng, S. Zou, X. Shuai, *Angew. Chem., Int. Ed.* **2011**, *50*, 9404.
[26] a) C. Huang, K. G. Neoh, L. Xu, E. T. Kang, E. Chiong, *Biomacromolecules* **2012**, *13*, 2513; b) V. T. Huynh, G. Chen, Pd. Souza, M. H. Stenzel, *Biomacromolecules* **2011**, *12*, 1738.
[27] X. Yang, S. Kootala, J. Hilborn, D. A. Ossipov, *Soft Matter* **2011**, *7*, 7517.
[28] S. Dufort, L. Sancey, J.-L. Coll, *Adv. Drug Delivery Rev.* **2012**, *64*, 179.
[29] Y. Li, H. He, X. Jia, W. L. Lu, J. Lou, Y. Wei, *Biomaterials* **2012**, *33*, 3899.
[30] Z. Wang, Y. Yu, W. Dai, J. Lu, J. Cui, H. Wu, L. Yuan, H. Zhang, X. Wang, J. Wang, X. Zhang, Q. Zhang, *Biomaterials* **2012**, *33*, 8451.
[31] K. Xiao, Y. Li, J. Luo, J. S. Lee, W. Xiao, A. M. Gonik, R. G. Agarwal, K. S. Lam, *Biomaterials* **2011**, *32*, 3435.
[32] a) R. Wei, L. Cheng, M. Zheng, R. Cheng, F. Meng, C. Deng, Z. Zhong, *Biomacromolecules* **2012**, *13*, 2429; b) D. M. Ren, M. Dalmau, A. Randall, M. M. Shindel, P. Baldi, S. W. Wang, *Adv. Funct. Mater.* **2012**, *22*, 3170.
[33] Y. Lee, R. Graeser, F. Kratz, K. E. Geckeler, *Adv. Funct. Mater.* **2011**, *21*, 4211.
[34] Y.-L. Li, L. Zhu, Z. Liu, R. Cheng, F. Meng, J.-H. Cui, S.-J. Ji, Z. Zhong, *Angew. Chem., Int. Ed.* **2009**, *48*, 9914.
[35] S. Ganta, H. Devalapally, A. Shahiwala, M. Amiji, *J. Controlled Release* **2008**, *126*, 187.
[36] L. Zhao, J. X. Ding, C. S. Xiao, P. He, Z. H. Tang, X. Pang, X. L. Zhuang, X. S. Chen, *J. Mater. Chem.* **2012**, *22*, 12319.
[37] Q. Xiao, W. Bu, Q. Ren, S. Zhang, H. Xing, F. Chen, M. Li, X. Zheng, Y. Hua, L. Zhou, W. Peng, H. Qu, Z. Wang, K. Zhao, J. Shi, *Biomaterials* **2012**, *33*, 7530.
[38] P. A. Ma, S. Liu, Y. B. Huang, X. S. Chen, L. P. Zhang, X. B. Jing, *Biomaterials* **2010**, *31*, 2646.
[39] A. L. Lee, S. Venkataraman, S. B. Sirat, S. Gao, J. L. Hedrick, Y. Y. Yang, *Biomaterials* **2012**, *33*, 1921.
[40] A. Bressenot, S. Marchal, L. Bezdetnaya, J. Garrier, F. Guillemin, F. Plenat, *J. Histochem. Cytochem.* **2009**, *57*, 289.

© 2013 WILEY-VCH Verlag GmbH & Co. KGaA, Weinheim